atmosphere

MDPI

Article

Comparative Study of Atmospheric Polycyclic Aromatic Hydrocarbons (PAHs) and Nitro-PAHs at Marine and Forest Background Stations in Shimane, Japan (2022–2024)

Yan Wang [1], Pengchu Bai [1], Xuan Zhang [2], Shingo Matsumoto [3], Tamon Yamashita [3], Masa-aki Yoshida [3], Seiya Nagao [4], Ammara Habib [5,6], Bushra Khalid [7], Lulu Zhang [4,8,9], Bin Chen [10,11,12,*] and Ning Tang [4,13,14,*]

1 Graduate School of Medical Sciences, Kanazawa University, Kanazawa 920-1192, Japan; wangyan@stu.kanazawa-u.ac.jp (Y.W.); baipengchu@stu.kanazawa-u.ac.jp (P.B.)
2 National Institute of Occupational Safety and Health, Japan Organization of Occupational Health and Safety, Kawasaki 214-8585, Japan; zhang-xuan@h.jniosh.johas.go.jp
3 Faculty of Life and Environmental Sciences, Shimane University, Matsue 690-8504, Japan; smatsu@life.shimane-u.ac.jp (S.M.); tamonyam@life.shimane-u.ac.jp (T.Y.); mayoshida@life.shimane-u.ac.jp (M.A.Y.)
4 Institute of Nature and Environmental Technology, Kanazawa University, Kanazawa 920-1192, Japan; seiya-nagao@se.kanazawa-u.ac.jp (S.N.); zhanglulu@hbut.edu.cn (L.Z.)
5 The Urban Unit, Lahore 54000, Pakistan; dr.ammara@urbanunit.gov.pk
6 International Center for Climate and Environment Sciences, Institute of Atmospheric Physics, Chinese Academy of Sciences, Beijing 100017, China
7 China-Pakistan Joint Research Center on Earth Sciences, Chinese Academy of Sciences and Higher Education Commission, Islamabad 45320, Pakistan; kh_bushra@yahoo.com
8 School of Civil Engineering, Architecture and Environment, Hubei University of Technology, Wuhan 430068, China
9 Key Laboratory of Intelligent Health Perception and Ecological Restoration of Rivers and Lakes, Ministry of Education, Hubei University of Technology, Wuhan 430068, China
10 Collaborative Innovation Center on Forecast and Evaluation of Meteorological Disasters, Nanjing University, Nanjing 210044, China
11 Institute of Atmospheric Physics, Chinese Academy of Sciences, Beijing 100029, China
12 Institute of Carbon Neutrality, Qilu Zhongke, Jinan 251401, China
13 Institute of Medical, Pharmaceutical and Health Sciences, Kanazawa University, Kanazawa 920-1192, Japan
14 College of Energy and Power, Shenyang Institute of Engineering, Shenyang 110136, China
* Correspondence: chen_bin@mail.iap.ac.cn (B.C.); n_tang@staff.kanazawa-u.ac.jp (N.T.); Tel.: +81-76-234-4455 (N.T.)

check for updates

Academic Editor: Pilar Fernández Ramón

Received: 15 October 2025
Revised: 13 November 2025
Accepted: 17 November 2025
Published: 20 November 2025

Citation: Wang, Y.; Bai, P.; Zhang, X.; Matsumoto, S.; Yamashita, T.; Yoshida, M.-a.; Nagao, S.; Habib, A.; Khalid, B.; Zhang, L.; et al. Comparative Study of Atmospheric Polycyclic Aromatic Hydrocarbons (PAHs) and Nitro-PAHs at Marine and Forest Background Stations in Shimane, Japan (2022–2024). *Atmosphere* **2025**, *16*, 1311. https://doi.org/10.3390/atmos16111311

Abstract

To clarify the pollution characteristics of polycyclic aromatic hydrocarbons (PAHs) and nitro-PAHs (NPAHs) in the East Asian monsoon region under different atmospheric environments and to assess their potential influences on receptor areas, this study selected two background monitoring stations with different environments in Shimane Prefecture, Japan: a marine station (MB) and a forest station (SF). $PM_{2.5}$ samples were simultaneously collected using a high-volume sampler during the summer and winter of 2022–2023, and ten PAHs and three NPAHs were quantified using HPLC. The concentrations of PAHs and NPAHs at MB and SF exhibited significant seasonal variations in 2022 (winter > summer). However, in 2023, a clear seasonal difference was observed only at MB. Isomer ratio analysis of PAHs at both stations indicated that traffic emissions and biomass or coal combustion were major contributors. Seasonal variations in the [2-NFR]/[1-NP] ratio indicated that, while high ratios at MB and SF during summer were mainly associated with local photochemical formation, low ratios in winter reflected long-range transportation of combustion-derived PAHs and NPAHs from the Asian continent. Incremental lifetime cancer risk values (10^{-7} to 10^{-11}) indicated that even at background stations, the atmospheric environment poses certain health risks. This first comparative investigation of PAHs and

NPAHs at two distinct background stations in Shimane again highlights the importance of international cooperation among East Asian countries for effective air pollution control.

Keywords: polycyclic aromatic hydrocarbons; nitro-polycyclic aromatic hydrocarbons; background monitoring station; East Asia; transboundary pollution

1. Introduction

Polycyclic aromatic hydrocarbons (PAHs) and nitro-polycyclic aromatic hydrocarbons (NPAHs) have long attracted attention because of their recognized carcinogenic, mutagenic, and teratogenic effects [1–5]. Atmospheric PAHs and NPAHs are mainly produced by the partial combustion of petroleum, coal, wood, and other organic materials. In urban regions, vehicles, factories, and thermal power plants are the major contributors to PAHs and NPAHs [6–8]. In rural regions, the contribution of biomass burning cannot be underestimated [9,10]. Through interactions with atmospheric oxidants like ozone (O_3), hydroxyl radicals (OH), and nitrogen oxides (NO_x), PAHs can be transformed into more toxic derivatives, such as NPAHs and quinones [11–13]. In remote areas, atmospheric transportation from upwind regions can sometimes lead to more complex changes in chemical composition [14,15].

During the past 40 years, intensified industrial growth and urban development across East Asia have significantly elevated PAH and NPAH emissions [16], although strict control measures have been implemented in recent years, significantly reducing emissions of PAHs and NPAHs in major East Asian countries such as China, Japan, and Republic of Korea [17–19]. East Asia remains one of the regions with the highest emission levels in the world [20,21]. According to recent studies, cities in northern China, such as Shenyang (18.7 ng/m^3), and Beijing (32.8 ng/m^3), exhibited relatively high concentrations of PAHs. The urban concentrations observed in Republic of Korea were comparatively lower (Seoul: 3.66 ng/m^3) but still higher than those in Japan (Kanazawa: 0.32 ng/m^3) [22–25]. Since these countries and regions all lie within the well-known East Asian monsoon zone, transboundary pollution of atmospheric pollutants during the peak periods of the monsoon has long been a well-recognized phenomenon [26,27]. Specifically, during the summer monsoon, air masses generally flow from the Pacific toward the Japanese archipelago and the southern regions of China, while in the winter, colder continental air masses from northern and northeastern Asia move toward Japan, often bringing pollutants from inland China, Mongolia, and the Russian Far East [28,29]. Our previous monitoring background stations on the Sea of Japan coast revealed that air masses originating from the Japanese mainland mainly affected the concentrations of PAHs and NPAHs. In contrast, during the winter monsoon, the influx of PAHs and NPAHs from the Asian continent caused concentrations to increase three- to tenfold [23,30]. Meanwhile, these investigations also revealed that for two geographically separated background stations facing the Asian continent (Wajima, Ishikawa Prefecture, and Fukue Island, Nagasaki Prefecture), the temporal and compositional variations in the concentrations of PAHs and NPAHs were not necessarily consistent during simultaneous observations [30,31]. It is inferred that the differences are mainly caused by variations in atmospheric pressure patterns. Therefore, to systematically understand the differing impacts of PAHs and NPAHs on receptor regions and to develop targeted environmental protection policies, it is essential to conduct background observations across different regions.

Shimane Prefecture, situated on Japan's western seaboard and facing the Asian continent across the Sea of Japan, lies geographically between the two background stations

investigated in our previous studies (Ishikawa and Nagasaki Prefectures) and is located approximately 350 km east of the Korean Peninsula. With a total population of 657,842, it ranks 46th nationwide. Its forest coverage rate of 78.7%, the third highest among all prefectures in Japan [32], highlights its significance for forest-related atmospheric studies. In addition, Shimane Prefecture, which possesses the longest coastline in Japan, extending approximately 640 km along the Sea of Japan, serves as a key receptor region within the East Asian monsoon area due to its geographical orientation toward the Asian continent [33–35].

Because the atmospheric behaviors of PAHs and NPAHs differ between marine and forest environments [36–38], this study, based on the geographical characteristics of Shimane Prefecture, conducted a two-year comparative investigation at a marine background station (MB) and a forest background station (SF). The concentrations, compositional characteristics, and potential sources of PAHs and NPAHs were compared to evaluate whether the influences of the East Asian summer and winter monsoons differ. The findings provide fundamental data for future atmospheric observation networks and environmental policy development.

2. Materials and Methods

2.1. Sample Collection

A total of 120 $PM_{2.5}$ samples were obtained during two consecutive summer–winter cycles: July to September 2022 and January to March 2023, followed by July to September 2023 and January to March 2024. Sampling was carried out at two background monitoring stations, Oki Marine Biological Station (MB, 36.19° N, 133.27° E) and Sambe Forest (SF, 35.17° N, 132.62° E), both operated by Shimane University (Figure 1). MB is located on the Oki Islands near Saigo Port and represents a typical marine background site. SF is situated on the main island of Honshu near Sanbecho Shigaku, Ota City, and is characterized as an inland forested background area. This geographical contrast provides a valuable framework for investigating the spatiotemporal distribution of atmospheric pollutants between coastal and inland environments.

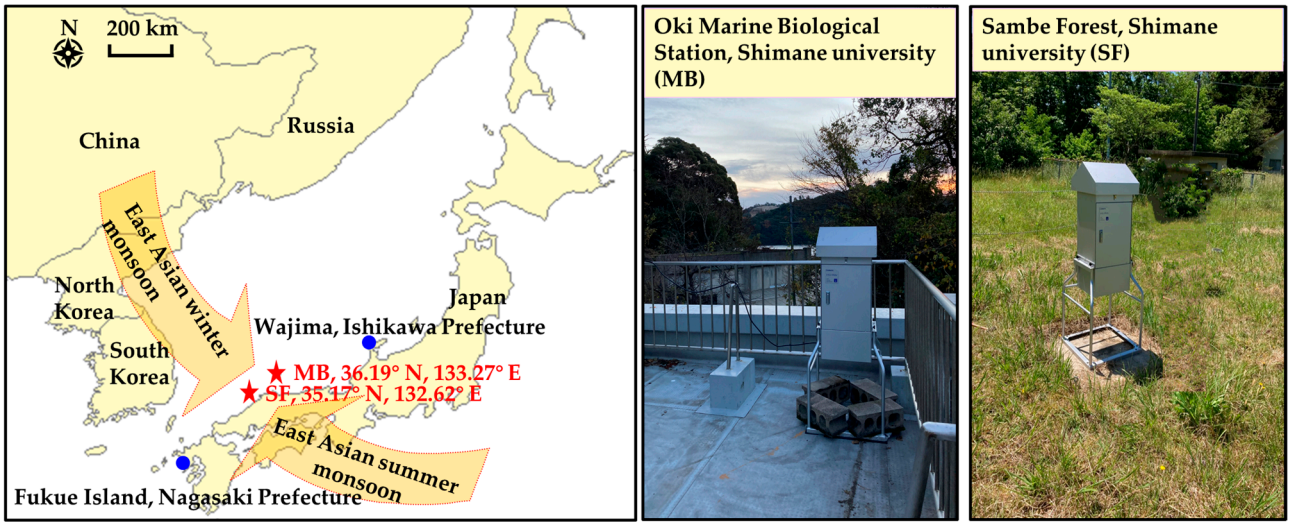

Figure 1. The location of sampling stations (the map was generated using MeteoInfo software 3.8.11, accessed on 30 October 2025).

Using a high-volume air sampler (Sibata Sci. Tech. Ltd., Saitama, Japan) fitted with quartz fiber filters (2500QAT-UP, Pallflex Products, Putnam, CT, USA), $PM_{2.5}$ was collected continuously for 24 h at a flow rate of 1000 L/min. Sampling was carried out on five successive days each month. After collecting, filters were conditioned in a desiccator for

72 h before being weighed, then wrapped in aluminum foil and stored at −27 °C until chemical analysis.

2.2. Chemicals

In each sample, ten PAH standards—including 4-ring PAHs: fluoranthene (FR), pyrene (Pyr), benzo[*a*]anthracene (BaA), chrysene (Chr); 5-ring PAHs: benzo[*b*]fluoranthene (BbF), benzo[*k*]fluoranthene (BkF), benzo[*a*]pyrene (BaP), benzo[*e*]pyrene (BeP); and 6-ring PAHs: benzo[*ghi*]perylene (BgPe), indeno[1,2,3-*cd*]pyrene (IDP)—were purchased from Supelco Park (Bellefonte, PA, USA). Three NPAHs—including 2-nitrofluoranthene (2-NFR) and 1-nitropyrene (1-NP)—were obtained from Aldrich Company Inc. (Milwaukee, WI, USA). 6-nitrobenzo[*a*]pyrene (6-NBaP) was obtained from AccuStandard, Inc. (New Haven, CT, USA). Pyr-d_{10} and BaP-d_{12} (Wako Pure Chemicals, Osaka, Japan) were used as surrogate standards for the quantification of PAHs, and 2-fluoro-7-nitrofluoranthenes (FNF, Aldrich Chemical Company, Milwaukee, WI, USA) were used as the internal standard for NPAHs (Wako Pure Chemicals, Osaka, Japan). All chemicals employed in this study were of analytical grade.

2.3. Sample Preparation and HPLC Analysis of PAHs and NPAHs

The pretreatment procedures, analytical protocols, and quality control processes followed in this study were aligned with our previous research [39,40]. $PM_{2.5}$ filters (17.8–103 cm^2) were cut, spiked with internal standards, extracted ultrasonically with dichloromethane, and concentrated for PAH and NPAH analysis. HPLC coupled with fluorescence and chemiluminescence detection was applied to quantify ten PAHs and three NPAHs following established procedures [39,40]; see Text S1 for details. The recovery rate of the indicator Pyr-d_{10} and BaP-d_{12} and FNF were 84 ± 12%, 118 ± 43%, and 94 ± 29%, respectively. Quality control was maintained by analyzing blank and reference standards after every seventh sample to verify accuracy and rule out contamination (Text S2 and Table S1). This also served to ensure robustness and reliability about the system of HPLC throughout the analytical process.

2.4. Statistical Analysis and Backwards Trajectory Clustering

2.4.1. Mann–Whitney U Test

To assess regional and seasonal variations in PAH and NPAH concentrations at MB and SF, a two-tailed Mann–Whitney U test was employed using R language (version 4.4.1). Effect sizes (r) were calculated to quantify the magnitude of group differences. A Bonferroni correction was applied to control for multiple comparisons across sampling sites and seasons. After correction, statistical significance was defined at $p < 0.05$. In Tables S2 and S3, the statistical test used, sample size, time coverage, and p-values are indicated.

2.4.2. Air-Mass Cluster Analysis Based on Backwards Trajectory Calculation

Air-mass backward trajectories during the sampling period were simulated using the MeteoInfo software 3.8.11 [41]. This model is widely employed for calculating air parcel trajectories and simulating the dispersion and deposition of atmospheric pollutants [42], based on meteorological data sets spanning various altitudes and time intervals [43]. The meteorological fields used in this study were retrieved from the Global Data Assimilation System (GDAS, ftp://arlftp.arlhq.noaa.gov/pub/archives/gdas1, accessed on 30 October 2025), supplied by the National Centers for Environmental Prediction (NCEP), NOAA Air Resources Laboratory (2025). In this study, 72 h backward air-mass trajectories were simulated for each sampling day during the summer and winter of 2022 and 2023 at MB and SF, with a starting height of 500 m above ground level (AGL). To ensure temporal consistency between the air-mass origin and the sampling period, the backward

trajectory analysis was initialized at the same time as the sampling. A total of 15 trajectories were obtained for each season (summer and winter) in 2022 and 2023 at MB and SF. The backward trajectories for the two stations during the summer and winter of 2022 and 2023 were clustered using the built-in clustering algorithm of the HYSPLIT model. The optimal number of clusters was determined based on the inflection point of the total spatial variance (TSV) curve [44]. Seasonal clustering diagrams were generated by grouping the backward trajectories using the HYSPLIT model's built-in clustering procedure.

2.5. Health Risk Assessment

According to the International Agency for Research on Cancer (IARC) classification of the carcinogenic potential of 16 priority PAHs, BaP is categorized as a Group 1 human carcinogen [45,46]. Therefore, the BaP toxic equivalent of individual PAHs is commonly used to assess cancer risk associated with PAH and NPAH emissions. BaP toxic equivalent is defined as the product of the concentration of each PAH and its toxic equivalency factor (TEQ). The TEF values for the PAHs and NPAHs used in this study were adopted from previous studies [47–49], which indicated that high-molecular-weight PAHs generally have higher TEF values compared to low- and medium-molecular-weight PAHs. The TEF values of 10 PAHs and 2 NPAHs used in this study are listed in Table S4 (Equations (1) and (2)).

The incremental lifetime cancer risk (ILCR) was combined with the toxic equivalency factor (TEF) model by Equations (3)–(6). ILCRs corresponding to ingestion, inhalation, and dermal absorption pathways, together with the total ILCR, were calculated as follows [50–52]: where TEQ_{total} is the sum of 10 individual PAHs and 2 NPAHs in pg m^{-3} and for ILCR calculations, TEQ_{total} values were converted to mg m^{-3} to maintain consistency with the units used in risk assessment equations. $ILCR_{ing}$, $ILCR_{inh}$, and $ILCR_{dem}$ denote the ILCR associated with ingestion, inhalation, and dermal adsorption, respectively. The carcinogenic slope factors (CSFs) for BaP were set as 7.3, 25, and 3.85 ((mg kg^{-1} $day^{-1})^{-1}$) for CSFing, CSFinh, and CSFdem, respectively [50,53]. Other parameters include BW, the mean body weight (kg) [54]; IRing, the ingestion rate (mg day^{-1}) [55]; EF, annual exposure frequency (days $year^{-1}$) [56]; ED, exposure duration (years) [56]; AT, the average lifespan (days) [56]; IRinh, inhalation rate (m^3 day^{-1}) [55]; PEF, the particle emission factor (m^3 kg^{-1}) [56]; SA, the exposed skin area (cm^2 day^{-1}) [56]; SF, the skin adherence factor (mg cm^{-2}) [55]; and ABS, the dermal absorption factor (day^{-1}) [55]. Comprehensive information on the parameters applied is presented in Table S5.

$$TEQ_i = C_i \times TEF_i \quad (1)$$

$$TEQ_{total} = \sum TEQ_i \quad (2)$$

$$ILCR_{ing} = TEQ_{total} \times CSF_{ing} \times \sqrt[3]{\frac{BW}{70}} \times IR_{ing} \times EF \times ED/(BW \times AT \times 10^6) \quad (3)$$

$$ILCR_{inh} = TEQ_{total} \times CSF_{inh} \times \sqrt[3]{\frac{BW}{70}} \times IR_{inh} \times EF \times ED/(BW \times AT \times PEF) \quad (4)$$

$$ILCR_{dem} = TEQ_{total} \times CSF_{dem} \times \sqrt[3]{\frac{BW}{70}} \times SA \times SF \times ABS \times EF \times ED/(BW \times AT \times 10^6) \quad (5)$$

$$\text{Total ILCR} = \text{ILCRing} + \text{ILCRinh} + \text{ILCR dem} \quad (6)$$

3. Results and Discussion

3.1. PAH and NPAH Concentrations

The median concentrations of PAHs and NPAHs measured in the atmosphere at both monitoring stations during summer and winter of 2022 and 2023 are shown in Figure 2. The median concentrations of various PAHs and NPAHs are shown in Table S6. In summer 2022, the median concentrations of PAHs and NPAHs were 74.53 pg m^{-3} and 0.37 pg m^{-3} at MB, and 67.43 pg m^{-3} and 0.58 pg m^{-3} at SF, respectively. In winter 2022, the PAH and NPAH median concentrations were 346.97 pg m^{-3} and 1.91 pg m^{-3} at MB, and 363.85 pg m^{-3} and 2.33 pg m^{-3} at SF, respectively. Seasonal variation was evident at both stations, with markedly reduced concentrations of PAHs and NPAHs in summer and significantly enhanced levels in winter ($p < 0.05$). And SF consistently exhibited slightly higher PAH and NPAH levels than MB. In summer 2023, the median PAH and NPAH concentrations were 50.94 pg m^{-3} and 0.36 pg m^{-3} at MB, and 340.28 pg m^{-3} and 1.78 pg m^{-3} at SF, respectively. In winter 2023, the median concentrations of PAHs and NPAHs were 267.09 pg m^{-3} and 1.52 pg m^{-3} at MB, and 249.54 pg m^{-3} and 2.18 pg m^{-3} at SF, respectively. This seasonal variation pattern differed from that observed in 2022. These results suggested that temporal variations in PAH and NPAH levels at the two background stations were governed by distinct factors.

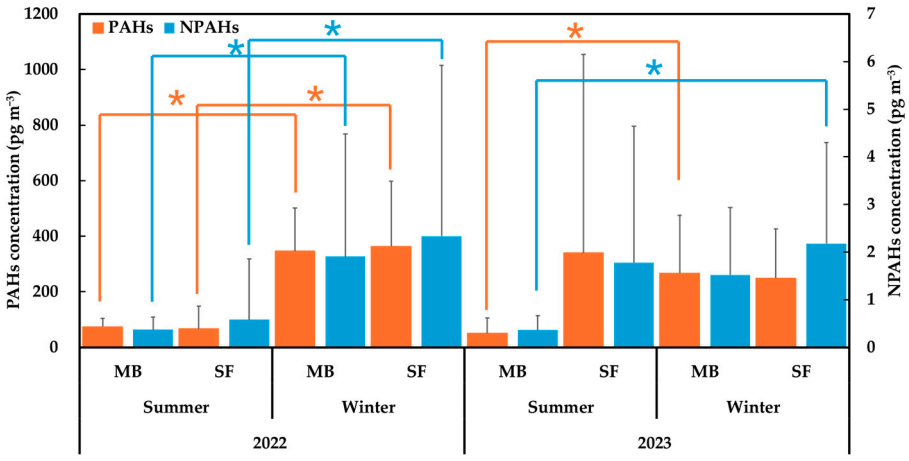

Figure 2. Median concentrations of PAHs and NPAHs at MB and SF in summer and winter of 2022 and 2023 (* indicates $p < 0.05$).

Compared with two other background stations located along the Sea of Japan, the Wajima monitoring station of Kanazawa University (KUWAMS) and the Fukue atmospheric and aerosol monitoring station (FAMS), the concentrations of nine PAHs (excluding BeP) in the atmosphere at MB and SF were higher than FAMS but comparable to those at KUWAMS in summer (Table S6). During winter, the concentrations observed at both MB and SF were lower than KUWAMS and FAMS [31].

3.2. Main Sources of PAHs and NPAHs

3.2.1. Primary Emission and Secondary Formation

Many studies have demonstrated that the composition of PAHs varies depending on fuel type and temperature during pyrolysis and combustion [18,57,58]. Therefore, molar concentration ratios of specific PAHs are widely employed to distinguish primary emission sources. As presented in Figure 3a, in both summers, [IDP]/([IDP] + [BgPe]) values at MB and SF ranged from 0.21 to 0.49, indicating that the primary source of PAHs was traffic emissions (0.20–0.50). Meanwhile, [FR]/([FR] + [Pyr]) values at MB and SF ranged from 0.10 to 0.64, suggesting that PAHs originated mainly from traffic emissions (<0.5) and

biomass or coal combustion (0.5–0.6). These results indicated that although both sources contributed to summer PAH concentrations at both stations to varying degrees, traffic emissions were the dominant source. In both winters, [IDP]/([IDP] + [BgPe]) ratios at MB and SF ranged from 0.21 to 0.39, still suggesting traffic emissions as the major origin of PAHs. However, in contrast to summer, most [FR]/([FR] + [Pyr]) values in winter were within the interval of 0.5 to 0.6, indicating a substantially higher contribution from biomass or coal combustion.

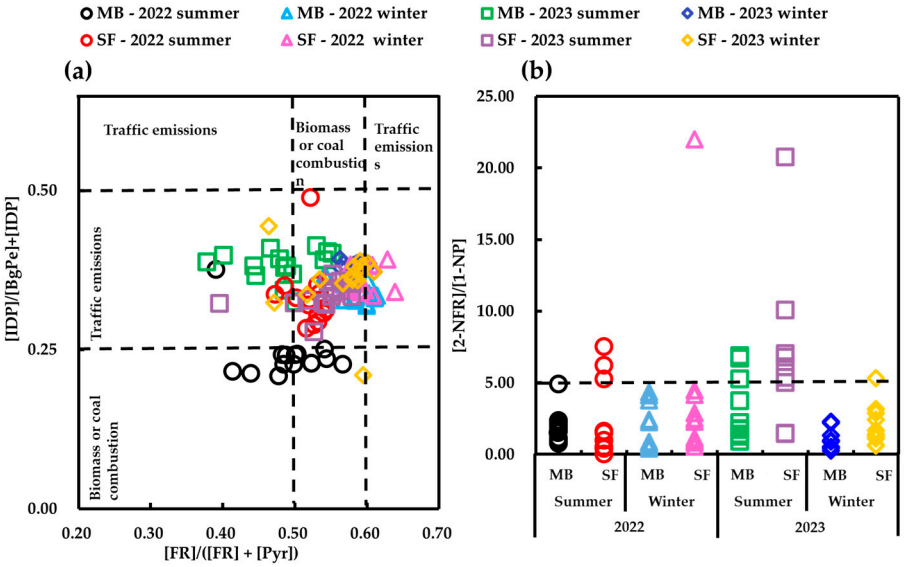

Figure 3. The distribution of PAHs and NPAHs ratios at MB and SF in summer and winter. (**a**) [BbF]/([BbF] + [BkF]) and [IDP]/([BgPe] + [IDP]); (**b**) [2-NFR]/([1-NP]).

For NPAHs, 2-NFR is a typical secondary species formed via the reaction of FR with OH radicals by day and with NO_3 radicals by night [59,60]. In contrast, 1-NP is mainly a primary pollutant directly emitted from combustion processes, particularly diesel exhaust. Therefore, [2-NFR]/[1-NP] ratio is commonly employed as an indicator of the atmospheric residence time of aerosol-associated PAHs and NPAHs, as well as the oxidation of the surrounding atmosphere. A [2-NFR]/[1-NP] ratio below 5 is generally interpreted to suggest that atmosphere-borne PAHs and NPAHs likely originate mainly from nearby sources or, if transported from other regions, have not undergone sufficient oxidation during transportation. In contrast, a ratio above 5 indicates that long-range atmospheric transportation may play a dominant role in PAH and NPAH pollution levels [30,61]. According to Figure 3b, the [2-NFR]/[1-NP] ratio values at MB and SF in both summers showed a wider distribution (MB: 0.26–6.89; SF: 0.42–21.98), including values below and above 5. It is noteworthy that days with [2-NFR]/[1-NP] ratios greater than 5 were consistently accompanied by elevated PAH concentrations. The specific locations and meteorological characteristics of the two background stations during summer (strong ultraviolet radiation and high humidity at MB, and strong ultraviolet radiation combined with high concentrations of biogenic VOCs at SF) favor the formation of OH radicals and other strong oxidants, as shown in Table S7 [62–64]. Therefore, unlike the results of previous investigations, it is possible that on days with high [2-NFR]/[1-NP] ratios at these characteristic background stations, the primary sources of PAHs and NPAHs were not long-range transportation but rather local specific activities.

In both winters, however, [2-NFR]/[1-NP] ratios at MB and SF were consistently below 5. Our previous research has shown that at KUWAMS, a background station also facing the Sea of Japan, the [2-NFR]/[1-NP] ratio values was also less than 5 during winter. This was ascribed to high concentrations of PAHs and NPAHs produced by combustion in northern China, together with secondarily formed 2-NFR, which were rapidly transported by strong

monsoon winds under conditions without limited further oxidation [61]. Therefore, the wintertime ratios below 5 at MB and SF may reflect similar regional transport influences, rather than being primary driven by local sources. This interpretation will be further discussed in the following section on long-range transportation, Section 3.2.2.

3.2.2. Long-Range Transportation

To better understand the environmental behavior of atmospheric contaminants in the East Asian monsoon region, we conducted long-term observations at background monitoring stations along the Sea of Japan coast. One key finding is that in winter, pollutants including PAHs and NPAHs, originating from heating devices and other sources on the Asian continent, are transported over long distances to these background stations under the influence of the Siberian high pressure. In contrast, in summer, the Pacific high pressure brings air masses from mainland Japan and the surrounding ocean, which have lower concentrations of PAHs and NPAHs, toward these stations [23,31].

Figure 4 presents the relationship between the daily concentrations of Σ(PAHs + NPAHs) and the cluster analysis of backward air-mass trajectories reaching MB and SF throughout the monitoring periods. As shown in Figure 4a, in the summer of 2022, 47% of the air masses arriving at MB were derived from the East China Sea and the Philippine Sea (Cluster 1), 20% from mainland Japan (Cluster 2), and 33% from the Sea of Japan (Cluster 3). In contrast, SF experienced a different transport pattern: 20% of the air masses originated from the East China Sea and the Philippine Sea (Cluster 1), 27% from domestic Japan (Cluster 2), and 53% from the Korean Peninsula (Cluster 3). According to the concentration data in the same figure (Figure 4a), the levels of PAHs and NPAHs at SF were higher than those at MB from 26 to 27 July 2022. During these days, the air masses reaching SF primarily originated from the Korean Peninsula (Cluster 3), while those arriving at MB were mainly of oceanic origin (Clusters 1 and 3), suggesting that the former may have transported more pollutants, whereas the latter reflected a relatively cleaner influence of marine air masses. However, not all air masses transported from the Korean Peninsula were associated with elevated PAH and NPAH concentrations. For example, on 18, 20–22, and 28 July 2022, PAH and NPAH levels at SF remained relatively low despite the dominance of Cluster 3. This indicated that the elevated concentrations observed on 26–27 July were likely influenced by local pollution events near SF. In the summer of 2023 (Figure 4c), all air masses arriving at MB were traced back to the Philippine Sea, the East China Sea, and mainland Japan (Clusters 1–3). For the same reason as in summer 2022, PAH and NPAH concentrations at MB remained low. At SF, however, 27% of air masses were transported from the Russian Far East (Cluster 1), due to a different sampling period compared to MB. Since these trajectories did not pass through highly polluted areas such as the Vladivostok Naval Base [29], no corresponding increase in pollutant levels was observed during 5–8 September. Interestingly, as in the previous year, peak concentrations of PAHs and NPAHs were again observed at SF in 2023, specifically during 21–22 August and 29–31 August. Air-mass cluster analysis indicated that the air masses during these periods mainly belonged to Clusters 2 and 3, both of which passed over mainland Japan. Simultaneously, the highest PAH and NPAH concentrations in SF were observed on 26–27 July 2022 (Figure 4a: Cluster 3) and 21–22 August 2023 (Figure 4b: Cluster 2). The common meteorological feature was the relatively slow wind speed, which made it difficult for accumulated atmospheric pollutants to diffuse. Unlike MB, SF is located in a mountainous area with dense forest cover and is known as a popular destination for summer tourism, camping, and outdoor cooking activities [65]. During both peak periods, the [FR]/([FR] + [Pyr]) ratio at SF ranged from 0.5 to 0.6, supporting the hypothesis that these peaks were related to enhanced emissions from local recreational activities.

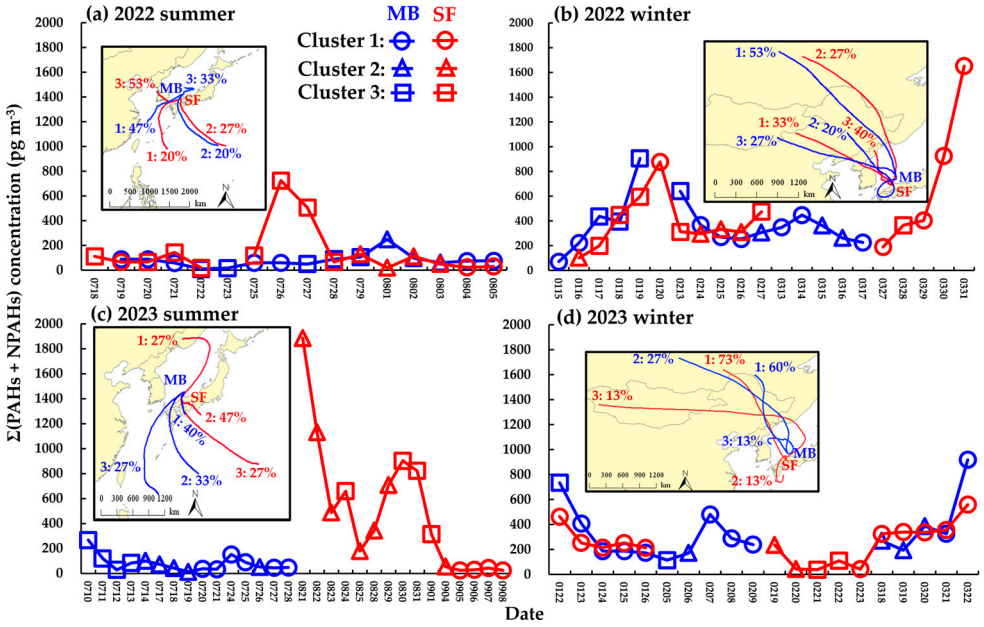

Figure 4. The temporal variation of Σ (PAHs + NPAHs) combined with air masses cluster analysis based on 72 h backward trajectory at MB and SF in summer and winter of 2022 and 2023.

In winter 2022 (Figure 4b), 53% of the air masses arriving at MB originated from central Russia and passed through northeastern China (Cluster 1), 20% came directly from northeastern China (Cluster 2), and 27% were transported from Mongolia via eastern China and the Korean Peninsula (Cluster 3). At SF, 33% of the air masses were from northeastern China (Cluster 1), 27% from central Russia via northeastern China (Cluster 2), and 40% from the Korean Peninsula (Cluster 3). Although there were some differences in transport routes, nearly all air masses during winter 2022 originated from or passed over the Asian continent. In fact, PAH and NPAH concentrations at MB and SF showed similar temporal variation during the overlapping sampling period. Peak concentrations occurred on 19 January at MB (Cluster 3) and 20 January at SF (Cluster 1), as well as on 31 March at SF (Cluster 1), with Clusters 3 at MB and 1 at SF following almost identical transport pathways. These results, which are consistent with our previous studies [23,31,61], suggested that wintertime PAHs and NPAHs at MB and SF were mainly attributed to long-range atmospheric transport from the Asian continent. In winter 2023 (Figure 4d), although approximately 13% of the air masses arriving at SF (Cluster 2) were from mainland Japan, and 13% of those reaching MB (Cluster 3) came from the coastal area of the Korean Peninsula, the dominant transport patterns still indicated Asian continental origins (MB: Cluster 1, 60%; Cluster 2, 27%. SF: Cluster 1, 73%; Cluster 3, 13%). As in winter 2022, PAH and NPAH concentrations at MB and SF exhibited similar temporal trends during the period of overlapping sampling. Therefore, the PAHs and NPAHs at the two stations in the winter of 2023 can also be explained as mainly originating from the Asian continent.

3.3. Health Effects of PAHs and NPAHs

Only 10 PAHs and 2 NPAHs were considered in the calculation of ∑TEQtotal (Table S8) because of the limited availability of TEF values. In both the summer and winter periods of 2022–2023, the ∑TEQtotal values of PAHs and NPAHs exhibited consistent site differences, with higher values at MB than at SF, except in summer 2023. This suggested that the concentrations of potentially carcinogenic PAHs and NPAHs were generally higher at MB than at SF. During the summer and winter of both years, the total ∑TEQtotal ranged from 0.77 to 278.79 pg/m^3, which is much lower than the standard value recommended by the WHO (1 ng/m^3). The ILCRs of PAHs and NPAHs via inhalation, ingestion, and dermal

contact exhibited spatial trends similar to those of ∑TEQtotal. In both seasons of 2022, the carcinogenic risk at MB was higher than at SF, whereas the opposite was observed in 2023 (Table 1).

Table 1. ILCR values of PAHs and NPAHs by three exposure pathways at MB and SF in summer and winter from 2022 to 2023.

		$ILCR_{ing}$	$ILCR_{inh}$	$ILCR_{dem}$	Total ILCR
MB-2022 summer	Male	4.74×10^{-8}	3.60×10^{-11}	1.05×10^{-8}	5.80×10^{-8}
	Female	5.40×10^{-8}	3.07×10^{-11}	1.19×10^{-8}	6.60×10^{-8}
SF-2022 summer	Male	3.31×10^{-8}	2.51×10^{-11}	7.32×10^{-9}	4.05×10^{-8}
	Female	3.77×10^{-8}	2.14×10^{-11}	8.33×10^{-9}	4.60×10^{-8}
MB-2022 winter	Male	2.18×10^{-7}	1.66×10^{-10}	4.83×10^{-8}	2.67×10^{-7}
	Female	2.48×10^{-7}	1.41×10^{-10}	5.49×10^{-8}	3.03×10^{-7}
SF-2022 winter	Male	1.30×10^{-7}	9.86×10^{-11}	2.87×10^{-8}	1.59×10^{-7}
	Female	1.48×10^{-7}	8.41×10^{-11}	3.27×10^{-8}	1.80×10^{-7}
MB-2023 summer	Male	2.04×10^{-8}	1.55×10^{-11}	4.51×10^{-9}	2.49×10^{-8}
	Female	2.32×10^{-8}	1.32×10^{-11}	5.13×10^{-9}	2.83×10^{-8}
SF-2023 summer	Male	1.67×10^{-7}	1.27×10^{-10}	4.21×10^{-8}	2.09×10^{-7}
	Female	1.90×10^{-7}	1.08×10^{-10}	4.79×10^{-8}	2.38×10^{-7}
MB-2023 winter	Male	9.52×10^{-8}	7.23×10^{-11}	2.10×10^{-8}	1.16×10^{-7}
	Female	1.08×10^{-7}	6.17×10^{-11}	2.39×10^{-8}	1.32×10^{-7}
SF-2023 winter	Male	9.54×10^{-8}	7.24×10^{-11}	2.11×10^{-8}	1.17×10^{-7}
	Female	1.09×10^{-7}	6.18×10^{-11}	2.40×10^{-8}	1.33×10^{-7}

Within the studied population, females exhibited greater potential cancer risks than males through ingestion and dermal pathways, whereas inhalation posed a comparatively higher risk. All total ILCR values remained below the acceptable standard recommended by the US EPA (1×10^{-6}), indicating that the concentrations of PAHs and NPAHs at MB and SF pose relatively low carcinogenic risks. It should be noted that 6-nitrofluoranthene, considered among the most potent carcinogenic NPAHs, was absent from detection in the present investigation, and 6-NBaP was excluded from the calculation due to the lack of TEF value. Among the three exposure pathways, ingestion and dermal contact were the dominant routes, posing carcinogenic risks that were 2–4 orders of magnitude higher than that of inhalation. Overall, although MB and SF are both background stations, potential health risks associated with PAHs and NPAHs remain.

4. Conclusions

This study provided a comparative characterization of the spatiotemporal behavior of PAHs and NPAHs over two consecutive years at two different types of background stations in Japan facing the Sea of Japan. Excluding temporary high concentrations caused by specific local events near the sampling sites, such as summer camping activities, no significant differences were observed in the atmospheric concentrations of PAHs and NPAHs between the two stations. Mixed sources of traffic emissions and biomass or coal combustion were identified in both summer and winter, with a stronger contribution from biomass or coal combustion during winter. The [2-NFR]/[1-NP] ratios at MB and SF suggested that local photochemical processes may have influenced summer conditions, while consistently low winter values were linked to long-range transportation of insufficiently oxidized pollutants from East Asia. Cluster analysis further indicated that clean marine air masses played a role in reducing concentrations at MB in summer, whereas local recreational activities may have contributed to elevated concentrations at SF. In winter, both stations exhibited similar variation patterns, primarily shaped by the East Asian continent. Despite the different

atmospheric settings at MB and SF, the East Asian summer and winter monsoons affected PAHs and NPAHs to a similar extent at both sites. Although the ILCR values ranged from 10^{-7} to 10^{-11}, implying relatively low levels, carcinogenic risks through all three exposure pathways were still present and warrant continued attention. To the best of our knowledge, this study represents the first comprehensive investigation of atmospheric PAHs and NPAHs conducted at two different typical background stations in Shimane Prefecture. The results provide reliable baseline data for understanding the mechanisms of long-range transport during the prevailing monsoon periods and for developing future transboundary pollution prediction models of PAHs and NPAHs under different synoptic pressure patterns. Furthermore, the findings underscore the critical importance of close international cooperation in controlling air pollution across the East Asian monsoon region.

Supplementary Materials: The following supporting information can be downloaded at: https://www.mdpi.com/article/10.3390/atmos16111311/s1, Text S1: Detailed experimental procedures for PAH and NPAH analysis; Text S2. Quality control and assurance; Table S1. Regression parameters (R^2 and equation), detection and quantification limits (LOD and LOQ), and linear ranges for ten PAHs and three NPAHs; Table S2. Summary of Wilcoxon rank-sum test results for PAH concentrations at MB and SF in summer and winter of 2022 and 2023. Table S3. Summary of Wilcoxon rank-sum test results for NPAH concentrations at MB and SF in summer and winter of 2022 and 2023. Table S4: Toxic equivalent factors (TEF) of PAHs and NPAHs; Table S5: Parameters used for the estimation of the incremental lifetime cancer risks (ILCRs); Table S6: Median concentrations of PAHs and NPAHs in $PM_{2.5}$ (pg m^{-3}) at MB and SF during summer and winter from 2022 to 2023, and at KUWAMS and FAMS in 2017 and 2019; Table S7. The meteorological parameters, and ozone concentration at MB and SF during summer and winter in 2022 and 2023; Table S8: TEQBap values (pg m^{-3}) calculated from PAHs and NPAHs at MB and SF in the winter of 2022 and the summer of 2023.

Author Contributions: Conceptualization, L.Z., B.C. and N.T.; methodology, Y.W.; software, Y.W.; validation, Y.W., P.B. and X.Z.; formal analysis, Y.W.; investigation, S.M., T.Y. and M.A.Y.; resources, S.N. and N.T.; data curation, Y.W.; writing—original draft preparation, Y.W.; writing—review and editing, Y.W., A.H. and B.K.; visualization, Y.W. and P.B.; supervision, L.Z., B.C. and N.T.; project administration, L.Z., B.C. and N.T.; funding acquisition, B.C. and N.T. All authors have read and agreed to the published version of the manuscript.

Funding: This research was funded by the Sasakawa Scientific Research Grant, The Japan Science Society, grant number 2024–3012; Aid for Scientific Research, the Ministry of Education, Culture, Sports, Science and Technology, Japan, grant number 24KF0222, 25K15477; Kanazawa University "SANTO" project 2023 and the cooperative research programs of Institute of Nature and Environmental Technology, Kanazawa University, Japan, grant number 21001, 22002, 23016, 25089.

Institutional Review Board Statement: Not applicable.

Informed Consent Statement: Not applicable.

Data Availability Statement: The original contributions presented in this study are included in the article. Further inquiries can be directed to the corresponding author.

Acknowledgments: We are grateful for the data support provided by the National Centers for Environmental Prediction (NCEP) and the NOAA Air Resources Laboratory, as well as for the use of the MeteoInfo software 3.8.11. We thank Hirotoshi Kasane, Yoshinobu Ozaki and Erika Kasai (Shimane University) for help sampling in Oki Islands and Sambe Forest.

Conflicts of Interest: The authors declare no conflicts of interest.

References

1. Rengarajan, T.; Rajendran, P.; Nandakumar, N.; Lokeshkumar, B.; Rajendran, P.; Nishigaki, I. Exposure to Polycyclic Aromatic Hydrocarbons with Special Focus on Cancer. *Asian Pac. J. Trop. Biomed.* **2015**, *5*, 182–189. [CrossRef]
2. Olsson, A.C.; Fevotte, J.; Fletcher, T.; Cassidy, A.; Mannetje, A.'t.; Zaridze, D.; Szeszenia-Dabrowska, N.; Rudnai, P.; Lissowska, J.; Fabianova, E.; et al. Occupational Exposure to Polycyclic Aromatic Hydrocarbons and Lung Cancer Risk: A Multicenter Study in Europe. *Occup. Environ. Med.* **2010**, *67*, 98–103. [CrossRef]
3. Wells, P.G.; McCallum, G.P.; Lam, K.C.H.; Henderson, J.T.; Ondovcik, S.L. Oxidative DNA Damage and Repair in Teratogenesis and Neurodevelopmental Deficits. *Birth Defects Res. Part C Embryo Today Rev.* **2010**, *90*, 103–109. [CrossRef] [PubMed]
4. Diggs, D.L.; Harris, K.L.; Rekhadevi, P.V.; Ramesh, A. Tumor Microsomal Metabolism of the Food Toxicant, Benzo(a)Pyrene, in ApcMin Mouse Model of Colon Cancer. *Tumor Biol.* **2012**, *33*, 1255–1260. [CrossRef]
5. Lin, H.; Xia, X.; Lin, Y. Characterization and application of exposure biomarkers of polycyclic aromatic hydrocarbons in diesel exhaust. *J. Environ. Occup. Med.* **2023**, *40*, 529–535. [CrossRef]
6. Fu, J.; Fang, T.; Gao, Y.; Wang, T.; Jia, Z.; Guo, D.; Mao, H. Emission Characteristic, Spatial Distribution, and Health Risk of Polycyclic Aromatic Compounds (PAHs, NPAHs, and OPAHs) from Light-Duty Gasoline and Diesel Vehicles Based on on-Road Measurements. *Sci. Total Environ.* **2024**, *941*, 173390. [CrossRef]
7. Li, W.; Wang, C.; Shen, H.; Su, S.; Shen, G.; Huang, Y.; Zhang, Y.; Chen, Y.; Chen, H.; Lin, N.; et al. Concentrations and Origins of Nitro-Polycyclic Aromatic Hydrocarbons and Oxy-Polycyclic Aromatic Hydrocarbons in Ambient Air in Urban and Rural Areas in Northern China. *Environ. Pollut.* **2015**, *197*, 156–164. [CrossRef] [PubMed]
8. Zhai, Y.; Yin, Z.; Zhao, X.; Zhang, J.; Zuo, R.; Wu, J.; Yang, J.; Teng, Y.; Wang, J. Polycyclic Aromatic Hydrocarbons (PAHs) in the Environment of Beijing, China: Levels, Distribution, Trends and Sources. *Hum. Ecol. Risk Assess. Int. J.* **2018**, *24*, 137–157. [CrossRef]
9. Chang, D.; Song, Y. Estimates of Biomass Burning Emissions in Tropical Asia Based on Satellite-Derived Data. *Atmos. Chem. Phys.* **2010**, *10*, 2335–2351. [CrossRef]
10. Zhang, B.; Peng, Z.; Lv, J.; Peng, Q.; He, K.; Xu, H.; Sun, J.; Shen, Z. Gas Particle Partitioning of PAHs Emissions from Typical Solid Fuel Combustions as Well as Their Health Risk Assessment in Rural Guanzhong Plain, China. *Toxics* **2023**, *11*, 80. [CrossRef]
11. Vione, D.; Maurino, V.; Minero, C.; Pelizzetti, E.; Harrison, M.A.J.; Olariu, R.-I.; Arsene, C. Photochemical Reactions in the Tropospheric Aqueous Phase and on Particulate Matter. *Chem. Soc. Rev.* **2006**, *35*, 441–453. [CrossRef] [PubMed]
12. Nováková, Z.; Novák, J.; Kitanovski, Z.; Kukučka, P.; Smutná, M.; Wietzoreck, M.; Lammel, G.; Hilscherová, K. Toxic Potentials of Particulate and Gaseous Air Pollutant Mixtures and the Role of PAHs and Their Derivatives. *Environ. Int.* **2020**, *139*, 105634. [CrossRef]
13. Abbas, I.; Badran, G.; Verdin, A.; Ledoux, F.; Roumié, M.; Courcot, D.; Garçon, G. Polycyclic Aromatic Hydrocarbon Derivatives in Airborne Particulate Matter: Sources, Analysis and Toxicity. *Environ. Chem. Lett.* **2018**, *16*, 439–475. [CrossRef]
14. Lammel, G.; Mulder, M.D.; Shahpoury, P.; Kukučka, P.; Lišková, H.; Přibylová, P.; Prokeš, R.; Wotawa, G. Nitro-Polycyclic Aromatic Hydrocarbons—Gas–Particle Partitioning, Mass Size Distribution, and Formation along Transport in Marine and Continental Background Air. *Atmos. Chem. Phys.* **2017**, *17*, 6257–6270. [CrossRef]
15. Li, Z.; Wang, Y.; Guo, J.; Zhao, C.; Cribb, M.C.; Dong, X.; Fan, J.; Gong, D.; Huang, J.; Jiang, M.; et al. East Asian Study of Tropospheric Aerosols and Their Impact on Regional Clouds, Precipitation, and Climate (EAST-AIRCPC). *J. Geophys. Res. Atmos.* **2019**, *124*, 13026–13054. [CrossRef]
16. Shen, H.; Huang, Y.; Wang, R.; Zhu, D.; Li, W.; Shen, G.; Wang, B.; Zhang, Y.; Chen, Y.; Lu, Y.; et al. Global Atmospheric Emissions of Polycyclic Aromatic Hydrocarbons from 1960 to 2008 and Future Predictions. *Environ. Sci. Technol.* **2013**, *47*, 6415–6424. [CrossRef]
17. Zhang, L.; Morisaki, H.; Wei, Y.; Li, Z.; Yang, L.; Zhou, Q.; Zhang, X.; Xing, W.; Hu, M.; Shima, M.; et al. PM2.5-Bound Polycyclic Aromatic Hydrocarbons and Nitro-Polycyclic Aromatic Hydrocarbons inside and Outside a Primary School Classroom in Beijing: Concentration, Composition, and Inhalation Cancer Risk. *Sci. Total Environ.* **2020**, *705*, 135840. [CrossRef] [PubMed]
18. Xing, W.; Yang, L.; Zhang, H.; Zhang, X.; Wang, Y.; Bai, P.; Zhang, L.; Hayakawa, K.; Nagao, S.; Tang, N. Variations in Traffic-Related Polycyclic Aromatic Hydrocarbons in PM2.5 in Kanazawa, Japan, after the Implementation of a New Vehicle Emission Regulation. *J. Environ. Sci.* **2022**, *121*, 38–47. [CrossRef]
19. Choi, E.; Lee, J.Y.; Kim, Y.P. Long-Term (1993–2018) Particulate Polycyclic Aromatic Hydrocarbons (PAHs) Concentration Trend in the Atmosphere of Seoul: Changes in Major Sources and Health Effects. *Atmos. Environ.* **2024**, *325*, 120418. [CrossRef]
20. Ji, D.; Gao, M.; Maenhaut, W.; He, J.; Wu, C.; Cheng, L.; Gao, W.; Sun, Y.; Sun, J.; Xin, J.; et al. The Carbonaceous Aerosol Levels Still Remain a Challenge in the Beijing-Tianjin-Hebei Region of China: Insights from Continuous High Temporal Resolution Measurements in Multiple Cities. *Environ. Int.* **2019**, *126*, 171–183. [CrossRef]

21. Kurokawa, J.; Ohara, T. Long-Term Historical Trends in Air Pollutant Emissions in Asia: Regional Emission Inventory in ASia (REAS) Version 3. *Atmos. Chem. Phys.* **2020**, *20*, 12761–12793. [CrossRef]
22. Zhang, H.; Zhang, X.; Wang, Y.; Bai, P.; Zhang, L.; Chen, L.; Han, C.; Yang, W.; Wang, Q.; Cai, Y.; et al. Factor Analysis of Recent Variations of Atmospheric Polycyclic Aromatic Hydrocarbons (PAHs) and 1-Nitropyrene (1-NP) in Shenyang, China from 2014 to 2020. *Atmos. Pollut. Res.* **2023**, *14*, 101900. [CrossRef]
23. Zhang, L.; Yang, L.; Kashiwakura, K.; Zhao, L.; Chen, L.; Han, C.; Nagao, S.; Tang, N. Autumn and Spring Observations of PM2.5-Bound Polycyclic Aromatic Hydrocarbons and Nitro-Polycyclic Aromatic Hydrocarbons in China and Japan. *Environ. Pollut.* **2024**, *343*, 123139. [CrossRef] [PubMed]
24. Shin, S.M.; Lee, J.Y.; Shin, H.J.; Kim, Y.P. Seasonal Variation and Source Apportionment of Oxygenated Polycyclic Aromatic Hydrocarbons (OPAHs) and Polycyclic Aromatic Hydrocarbons (PAHs) in PM2.5 in Seoul, Korea. *Atmos. Environ.* **2022**, *272*, 118937. [CrossRef]
25. Zhang, X.; Zhang, H.; Wang, Y.; Bai, P.; Zhang, L.; Toriba, A.; Nagao, S.; Suzuki, N.; Honda, M.; Wu, Z.; et al. Estimation of Gaseous Polycyclic Aromatic Hydrocarbons (PAHs) and Characteristics of Atmospheric PAHs at a Traffic Site in Kanazawa, Japan. *J. Environ. Sci.* **2025**, *149*, 57–67. [CrossRef] [PubMed]
26. Bian, J.; Li, D.; Bai, Z.; Li, Q.; Lyu, D.; Zhou, X. Transport of Asian Surface Pollutants to the Global Stratosphere from the Tibetan Plateau Region during the Asian Summer Monsoon. *Natl. Sci. Rev.* **2020**, *7*, 516–533. [CrossRef]
27. Dahari, N.; Muda, K.; Latif, M.T.; Hussein, N. Studies of Atmospheric PM2.5 and Its Inorganic Water Soluble Ions and Trace Elements around Southeast Asia: A Review. *Asia-Pac. J. Atmos Sci.* **2021**, *57*, 361–385. [CrossRef]
28. Wang, Y.; Zhang, H.; Zhang, X.; Bai, P.; Neroda, A.; Mishukov, V.F.; Zhang, L.; Hayakawa, K.; Nagao, S.; Tang, N. PM-Bound Polycyclic Aromatic Hydrocarbons and Nitro-Polycyclic Aromatic Hydrocarbons in the Ambient Air of Vladivostok: Seasonal Variation, Sources, Health Risk Assessment and Long-Term Variability. *Int. J. Environ. Res. Public Health* **2022**, *19*, 2878. [CrossRef]
29. Yang, L.; Zhang, L.; Chen, L.; Han, C.; Akutagawa, T.; Endo, O.; Yamauchi, M.; Neroda, A.; Toriba, A.; Tang, N. Polycyclic Aromatic Hydrocarbons and Nitro-Polycyclic Aromatic Hydrocarbons in Five East Asian Cities: Seasonal Characteristics, Health Risks, and Yearly Variations. *Environ. Pollut.* **2021**, *287*, 117360. [CrossRef] [PubMed]
30. Yang, L.; Zhou, Q.; Zhang, H.; Zhang, X.; Xing, W.; Wang, Y.; Bai, P.; Yamauchi, M.; Chohji, T.; Zhang, L.; et al. Atmospheric Behaviour of Polycyclic and Nitro-Polycyclic Aromatic Hydrocarbons and Water-Soluble Inorganic Ions in Winter in Kirishima, a Typical Japanese Commercial City. *Int. J. Environ. Res. Public Health* **2021**, *18*, 688. [CrossRef]
31. Yang, L.; Zhang, L.; Zhang, H.; Zhou, Q.; Zhang, X.; Xing, W.; Takami, A.; Sato, K.; Shimizu, A.; Yoshino, A.; et al. Comparative Analysis of PM2.5-Bound Polycyclic Aromatic Hydrocarbons (PAHs), Nitro-PAHs (NPAHs), and Water-Soluble Inorganic Ions (WSIIs) at Two Background Sites in Japan. *Int. J. Environ. Res. Public Health* **2020**, *17*, 8224. [CrossRef]
32. Statistics Bureau of Japan. Available online: https://www.e-stat.go.jp/en/dbview?sid=0002073240 (accessed on 14 October 2025).
33. Hase, H.; Yoon, J.-H.; Koterayama, W. The Current Structure of the Tsushima Warm Current along the Japanese Coast. *J. Oceanogr.* **1999**, *55*, 217–235. [CrossRef]
34. Ito, M.; Morimoto, A.; Watanabe, T.; Katoh, O.; Takikawa, T. Tsushima Warm Current Paths in the Southwestern Part of the Japan Sea. *Prog. Oceanogr.* **2014**, *121*, 83–93. [CrossRef]
35. Senjyu, T.; Enomoto, H.; Matsuno, T.; Matsui, S. Interannual Salinity Variations in the Tsushima Strait and Its Relation to the Changjiang Discharge. *J. Oceanogr.* **2006**, *62*, 681–692. [CrossRef]
36. Zhang, H.; Zhang, Z.; Lin, W.; Lin, G.; Luo, C.; Fang, T.; Luo, N.; Cai, M.; Wang, L.; Yan, B.; et al. Disentangling Seasonal Dynamics and Transboundary Transport of PAHs in a Coastal Monsoon City. *Atmos. Res.* **2025**, *330*, 108613. [CrossRef]
37. Perala-Dewey, J.; Orr, K.; Hageman, K.J.; Zawar-Reza, P.; Shahpoury, P. Atmospheric Transport of Polycyclic Aromatic Hydrocarbons into Three Alpine Valleys: Influence of Local-Scale Wind Patterns and Chemical Partitioning. *Environ. Sci. Technol.* **2023**, *57*, 13114–13123. [CrossRef]
38. Arias, A.H.; Pozo, K.A.; Álvarez, M.B.; Pribylová, P.; Tombesi, N.B. Atmospheric PAHs in Rural, Urban, Industrial and Beach Locations in Buenos Aires Province, Argentina: Sources and Health Risk Assessment. *Environ. Geochem. Health* **2022**, *44*, 2419–2433. [CrossRef]
39. Tang, N.; Tokuda, T.; Izzaki, A.; Tamura, K.; Ji, R.; Zhang, X.; Dong, L.; Kameda, T.; Toriba, A.; Hayakawa, K. Recent Changes in Atmospheric Polycyclic Aromatic Hydrocarbons (PAHs) and Nitropolycyclic Aromatic Hydrocarbons (NPAHs) in Shenyang, China. *Environ. Forensics* **2011**, *12*, 342–348. [CrossRef]
40. Hayakawa, K. Environmental Behaviors and Toxicities of Polycyclic Aromatic Hydrocarbons and Nitropolycyclic Aromatic Hydrocarbons. *Chem. Pharm. Bull.* **2016**, *64*, 83–94. [CrossRef] [PubMed]
41. Wang, Y.Q. MeteoInfo: GIS Software for Meteorological Data Visualization and Analysis. *Meteorol. Appl.* **2014**, *21*, 360–368. [CrossRef]

42. Teggi, S.; Costanzini, S.; Ghermandi, G.; Malagoli, C.; Vinceti, M. A GIS-Based Atmospheric Dispersion Model for Pollutants Emitted by Complex Source Areas. *Sci. Total Environ.* **2018**, *610–611*, 175–190. [CrossRef]
43. Colston, J.M.; Ahmed, T.; Mahopo, C.; Kang, G.; Kosek, M.; de Sousa Junior, F.; Shrestha, P.S.; Svensen, E.; Turab, A.; Zaitchik, B. Evaluating Meteorological Data from Weather Stations, and from Satellites and Global Models for a Multi-Site Epidemiological Study. *Environ. Res.* **2018**, *165*, 91–109. [CrossRef]
44. Su, L.; Yuan, Z.; Fung, J.C.H.; Lau, A.K.H. A Comparison of HYSPLIT Backward Trajectories Generated from Two GDAS Datasets. *Sci. Total Environ.* **2015**, *506–507*, 527–537. [CrossRef]
45. Delistraty, D. Toxic Equivalency Factor Approach for Risk Assessment of Polycyclic Aromatic Hydrocarbons. *Toxicol. Environ. Chem.* **1997**, *64*, 81–108. [CrossRef]
46. IARC. *Working Group on the Evaluation of Carcinogenic Risks to Humans, International Agency for Research on Cancer*; Diesel and Gasoline Engine Exhausts and Some Nitroarenes (Vol. 46); World Health Organization: Geneva, Switzerland, 1989.
47. Collins, J.F.; Brown, J.P.; Alexeeff, G.V.; Salmon, A.G. Potency Equivalency Factors for Some Polycyclic Aromatic Hydrocarbons and Polycyclic Aromatic Hydrocarbon Derivatives. *Regul. Toxicol. Pharmacol.* **1998**, *28*, 45–54. [CrossRef] [PubMed]
48. Nisbet, I.C.T.; LaGoy, P.K. Toxic Equivalency Factors (TEFs) for Polycyclic Aromatic Hydrocarbons (PAHs). *Regul. Toxicol. Pharmacol.* **1992**, *16*, 290–300. [CrossRef] [PubMed]
49. U.S. EPA. *Environmental Protection Agency (EPA) Decontamination Research and Development Conference*; U.S. Environmental Protection Agency: Washington, DC, USA, 2010.
50. Chen, S.-C.; Liao, C.-M. Health Risk Assessment on Human Exposed to Environmental Polycyclic Aromatic Hydrocarbons Pollution Sources. *Sci. Total Environ.* **2006**, *366*, 112–123. [CrossRef]
51. Famiyeh, L.; Chen, K.; Xu, J.; Sun, Y.; Guo, Q.; Wang, C.; Lv, J.; Tang, Y.-T.; Yu, H.; Snape, C.; et al. A Review on Analysis Methods, Source Identification, and Cancer Risk Evaluation of Atmospheric Polycyclic Aromatic Hydrocarbons. *Sci. Total Environ.* **2021**, *789*, 147741. [CrossRef] [PubMed]
52. Dinis, M.d.L.; Fiuza, A. Methodology for Exposure and Risk Assessment in Complex Environmental Pollution Situations. In *Exposure and Risk Assessment of Chemical Pollution—Contemporary Methodology*; NATO Science for Peace and Security Series C: Environmental Security; Springer: Dordrecht, The Netherlands, 2009. [CrossRef]
53. Pongpiachan, S.; Hattayanone, M.; Suttinun, O.; Khumsup, C.; Kittikoon, I.; Hirunyatrakul, P.; Cao, J. Assessing Human Exposure to PM10-Bound Polycyclic Aromatic Hydrocarbons during Fireworks Displays. *Atmos. Pollut. Res.* **2017**, *8*, 816–827. [CrossRef]
54. Statistal Information of Shimane. Available online: https://pref.shimane-toukei.jp/index.php?view=4346; (accessed on 16 November 2025).
55. Taghon, G.L. Beyond Selection: Optimal Ingestion Rate as a Function of Food Value. *Am. Nat.* **1981**, *118*, 202–214. [CrossRef]
56. Armstrong, B.; Hutchinson, E.; Unwin, J.; Fletcher, T. Lung Cancer Risk after Exposure to Polycyclic Aromatic Hydrocarbons: A Review and Meta-Analysis. *Environ. Health Perspect.* **2004**, *112*, 970–978. [CrossRef]
57. Stogiannidis, E.; Laane, R. Source Characterization of Polycyclic Aromatic Hydrocarbons by Using Their Molecular Indices: An Overview of Possibilities. In *Reviews of Environmental Contamination and Toxicology*; Whitacre, D.M., Ed.; Springer International Publishing: Cham, Switzerland, 2015; pp. 49–133, ISBN 978-3-319-10638-0.
58. Chen, Y.-P.; Zeng, Y.; Guan, Y.-F.; Huang, Y.-Q.; Liu, Z.; Xiang, K.; Sun, Y.-X.; Chen, S.-J. Particle Size-Resolved Emission Characteristics of Complex Polycyclic Aromatic Hydrocarbon (PAH) Mixtures from Various Combustion Sources. *Environ. Res.* **2022**, *214*, 113840. [CrossRef]
59. Ramdahl, T.; Zielinska, B.; Arey, J.; Atkinson, R.; Winer, A.M.; Pitts, J.N. Ubiquitous Occurrence of 2-Nitrofluoranthene and 2-Nitropyrene in Air. *Nature* **1986**, *321*, 425–427. [CrossRef]
60. Arey, J.; Zielinska, B.; Atkinson, R.; Winer, A.M.; Ramdahl, T.; Pitts, J.N. The Formation of Nitro-PAH from the Gas-Phase Reactions of Fluoranthene and Pyrene with the OH Radical in the Presence of NOx. *Atmos. Environ. (1967)* **1986**, *20*, 2339–2345. [CrossRef]
61. Tang, N.; Sato, K.; Tokuda, T.; Tatematsu, M.; Hama, H.; Suematsu, C.; Kameda, T.; Toriba, A.; Hayakawa, K. Factors Affecting Atmospheric 1-, 2-Nitropyrenes and 2-Nitrofluoranthene in Winter at Noto Peninsula, a Remote Background Site, Japan. *Chemosphere* **2014**, *107*, 324–330. [CrossRef] [PubMed]
62. Singh, H.B.; Salas, L.J.; Chatfield, R.B.; Czech, E.; Fried, A.; Walega, J.; Evans, M.J.; Field, B.D.; Jacob, D.J.; Blake, D.; et al. Analysis of the Atmospheric Distribution, Sources, and Sinks of Oxygenated Volatile Organic Chemicals Based on Measurements over the Pacific during TRACE-P. *J. Geophys. Res. Atmos.* **2004**, *109*, D15. [CrossRef]
63. Rohrer, F.; Berresheim, H. Strong Correlation between Levels of Tropospheric Hydroxyl Radicals and Solar Ultraviolet Radiation. *Nature* **2006**, *442*, 184–187. [CrossRef]

64. Taraborrelli, D.; Lawrence, M.G.; Crowley, J.N.; Dillon, T.J.; Gromov, S.; Groß, C.B.M.; Vereecken, L.; Lelieveld, J. Hydroxyl Radical Buffered by Isoprene Oxidation over Tropical Forests. *Nat. Geosci.* **2012**, *5*, 190–193. [CrossRef]
65. Oda City Japan Heritage Promotion Council. Mt. Sanbe—Iwami Volcano Story 20. KAZAN STORY. Available online: https://www.iwami-kazan.jp/en/story/story20/ (accessed on 16 November 2025).